ACS OMEGA

Open Access

http://pubs.acs.org/journal/acsodf

Article

Metal-Encapsulated, Polymer-Containing Halide Salt Composites as Potential Long-Term Hosts for Radioiodine: Evaluating Halmets, Polyhalmets, and Halcermets

Brian J. Riley,* Nathan L. Canfield, Saehwa Chong, and Jarrod V. Crum

Cite This: *ACS Omega* 2024, 9, 34661−34674

Read Online

ACCESS | Metrics & More | Article Recommendations | Supporting Information

ABSTRACT: This paper presents composite waste form concepts for radioiodine immobilization including halide-metal (*halmet*) composites, polymer-halide-metal (*polyhalmet*) composites, and halide-ceramic-metal (*halcermet*) composites with data from experiments to evaluate these ideas. The encapsulant metal of choice for the pellets was Bi^0, and a cold-press-and-sinter approach was used for creating the pellets. A polymer (i.e., polyacrylonitrile or PAN) phase was included in some composite forms because this porous, passive polymer is used as a host matrix for active chemisorption-based getters. Metals of Ag^0, Bi^0, and Cu^0 were separately embedded into PAN beads, which were loaded with iodine in static tests. Included are details of experiments where PAN removal from the iodine-loaded composite beads was evaluated to reduce the overall volume of the final waste requiring immobilization and to improve the thermal stability of the final composite form. While these experiments demonstrate new concepts for radioiodine immobilization, more work is needed to fully understand the limitations of these approaches and further optimizations are needed before implementation at larger scales is feasible.

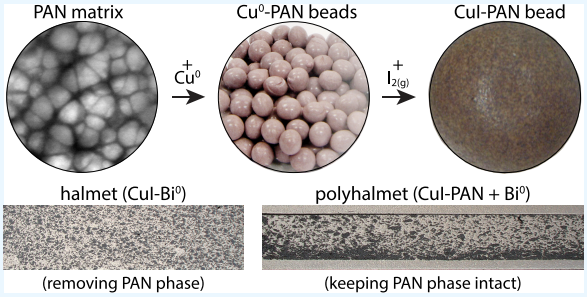

1. INTRODUCTION

With the ever-growing demand for energy across the world, nuclear power production remains one of the safest options, and it comes with a low carbon footprint.[1] Effective immobilization of radionuclides generated during nuclear processes is a high priority for both the environment and the safety of future generations. This includes capture of volatile radionuclides such as ^{129}I, ^{85}Kr, ^{14}C, and ^{3}H.[2] This paper focuses on the capture and long-term immobilization of radioiodine released from nuclear processes, which includes the high-activity, short-lived ^{131}I ($t_{1/2}$ = 8.02 days) and the low-activity, long-lived ^{129}I ($t_{1/2}$ = 1.57 × 10^7 years). Iodine is highly mobile in the environment[3] and can lead to thyroid cancer, so mitigating its release is essential.[4,5] Also, iodine speciation differs significantly across various streams and processes, including $I_{2(g)}$, $CH_3(CH_2)_xI$ (e.g., x = 0−11), ICl (iodine monochloride), HI, HOI, I^-, and IO_3^-.[2,6,7] This complicates the complete capture process using a single capture technology.

Liquid scrubbing is a general technology category for capturing radioiodine from off-gas streams and includes aqueous caustic scrubbing,[8−11] electrolytic scrubbing,[10,11] Iodox,[9,12] Mercurex,[8,9,13] and nonaqueous molten hydroxide.[14,15] An alternative approach to liquid scrubbing is to use a solid sorbent bed where the gaseous iodine species can be chemisorbed and selectively removed from the stream. The most common solid sorbents documented in the literature are Ag-containing materials (e.g., Ag-zeolites, Ag-silica, Ag-alumina),[16−29] but other metals have been receiving attention as well (e.g., Bi, Cu).[30−39]

Following radioiodine capture, the new stream or loaded solid sorbent will require immobilization, which includes concepts whereby the iodine-containing compounds are converted into a waste form suitable for long-term storage. The main goals in this step are minimizing waste volume by maximizing the density of the final form, maximizing the waste loading, and creating a chemically durable product. For caustic scrubber solutions, options include converting the mixture into halide-containing mineral waste forms[40] such as forms of sodalite [e.g., $Na_8(AlSiO_4)_6I_2$][23,41] or apatite [e.g., $Pb_{(10-x)}Ca_x(VO_4)_6I_2$, $Pb_{10}(VO_4)_{(6-y)}(PO_4)_yI_2$][41−44] through low-temperature processing[45] or hydrothermal processing.[46] For solid−sorbents, direct consolidation of the sorbent bed can be done with hot-pressing technologies such as hot isostatic pressing (HIP)[21,47−51] or spark plasma sintering (SPS)[27] whereby the porous sorbent structure will encapsulate the metal-iodide (MI_x) compound, which can result in changes to

Received: April 8, 2024
Revised: June 19, 2024
Accepted: July 31, 2024
Published: August 5, 2024

phase distribution, e.g., sodalite can be produced.[47] This consolidation process creates a double boundary against release and increases the resilience of iodine containment. Other options that have been explored include encapsulating the sorbent in a glassy phase through a glass-bonding technique to create a multiphase waste form,[51−53] or by using the encapsulating phase to create a glass-composite material (GCM) with the primary material as the core and the encapsulating matrix as a safety envelope around the core.[54] It should be noted that water-containing streams will likely require a calcination step prior to any sort of hot-pressing for waste form production.[55]

Another option for the multiphase encapsulation method includes using the HIP container or an additional protective layer (just inside the HIP container) as the envelope.[56,57] These additional boundary layers better encapsulate the core material, whereby the HIP process would compress the composite resulting in a denser multiphase waste form. The resulting product of encapsulating a MI_x compound within a metal matrix could be referred to as a halide-metal (*halmet*) composite, which has been described as a potential waste form option for immobilizing salt waste streams from nuclear processes, e.g., chlorides or fluorides from molten salt reactors[15,58] or chloride wastes from electrochemical reprocessing.[59] If a ceramic phase (e.g., zeolite-like composition) remains in the matrix, the resulting product could be referred to as a *halide-cermet composite*, *ceramic-halmet composite*, *halcermet*, or some other variation thereof. If the original sorbent contained a polymer phase such as polyacrylonitrile (PAN), which has been used for many promising off-gas capture technologies,[30,39,60−65] and this was encapsulated in a metal matrix as described above, the resulting composite waste form could be referred to as a *polyhalmet*, a *polycermet*,[66,67] or possibly a *polycerhalmet*, depending on the types of phases present (see Figure 1a,b).[68] Considering these multiphase waste forms, the goal in all cases is to maximize the MI_x content as shown by the "target region" designations in the phase diagrams (see Figure 1c,d).

Due to the low-temperature stability of PAN with a melting temperature (T_m) of 317 °C and a decomposition temperature (T_d) reported as low as 175 °C,[69] encapsulation processes for PAN-containing materials must be done using low-T_m encapsulant metals, which include Bi^0 (T_m = 271 °C), Bi^0-Sn^0 alloys (e.g., 58Bi-42Sn eutectic, T_m = 138 °C), Bi^0-Pb^0 alloys (e.g., 55.5Bi-44.5Pb eutectic, T_m = 124 °C), and Sn^0 (T_m = 231.93 °C).[70−72] The secondary advantage to utilizing Bi^0 and Pb^0 is that, if iodine is released from the initial sorbent material, these metals form MI_x compounds that are chemically and thermally stable (not the case with SnI_4). The possible MI_x compounds that could form with these metal encapsulants, in the event that iodine was released from the primary sorbent, include AgI (T_m = 558 °C), BiI_3 (T_m = 408.6 °C), BiOI (T_m = 308 °C), CuI (T_m = 591 °C), and PbI_2 (T_m = 410 °C). These data are summarized in Table 1 in addition to the boiling temperature (T_b), the bulk density (ρ_b), the solubility product constant (K_{sp}), and the waste loading of iodine (WL_I, mass%) for the potential MI_x compounds.[71] SnI_4 (T_m = 144 °C) is not suitable for iodine capture as the T_m is relatively low compared to other MI_x compounds, the T_m is below the expected operating temperature for a typical off-gas capture system (~150 °C), and it is not chemically durable.[73] As for BiI_3, phase transformation to BiOI can occur and release $I_{2(g)}$, but if

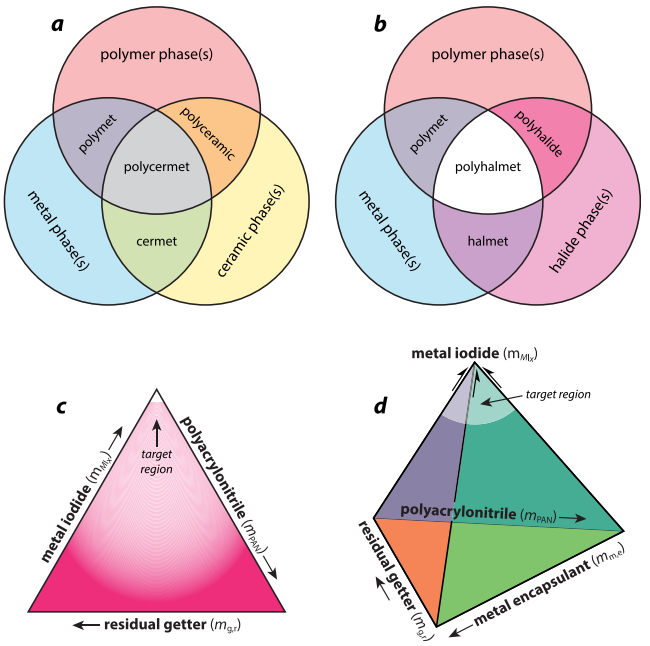

Figure 1. (a, b) Venn diagrams showing phase relationships and composite names for (a) the polymer−metal-ceramic material system and (b) the polymer−metal-halide material system. (c) Ternary diagram for mass loadings of the metal iodide (m_{MI_x}), the polymer (PAN) phase (m_{PAN}), and the residual getter phase ($m_{g,r}$) as well as (d) the quaternary system with the same phases as the ternary but with the added phase of additional metal encapsulant phase ($m_{m,e}$). For (c) and (d), the target regions are where the MI_x content is maximized.

Table 1. Summary of Metal-Iodide Compounds (MI_x) Including the Melting Temperatures (T_m), Boiling Temperatures (T_b), Bulk Densities (ρ_b), Solubility Product Constants (K_{sp}), and Iodine Waste Loading (WL_I) for Each Where Data Were Available[71]

MI_x	T_m (°C)	T_b (°C)	ρ_b(g/cm^3)	K_{sp}	WL_I (mass %)
AgI	558	1506	5.68	8.52×10^{-17}	54.1
BiI_3	408.6	542	5.778	7.71×10^{-19}	64.6
BiOI	308[a]	-	7.92	-	36.1
CuI	591	≈1290	5.67	1.27×10^{-12}	66.6
PbI_2	410	872[a]	6.16	9.5×10^{-9}	55.1

[a]Material decomposes.

BiI_3 is encapsulated within the durable matrix, iodine release can be mitigated.[73]

Since having PAN present in the sample leads to thermal limits for the consolidation process due to the low T_d of PAN, removing the PAN phase prior to decomposition would make the consolidation process more flexible. It also removes the concerns of unwanted reactions between the polymer phase and the other phases as well as the unknown degradation properties of the polymer phase over long time periods. Thus, during the course of this work, a process was proposed for removing the PAN matrix phase with dimethyl sulfoxide (DMSO) after iodine loading of PAN composite sorbents, i.e., isolating of PAN. It also removes the concerns of unwanted reactions between the polymer phase and the other phases as well as the unknown degradation properties of the polymer phase over long time periods. Thus, during the course of this work, a process was proposed for removing the PAN matrix

https://doi.org/10.1021/acsomega.4c03378
ACS Omega 2024, 9, 34661−34674

phase with dimethyl sulfoxide (DMSO) after iodine loading of PAN composite sorbents, i.e., isolating MI_x from the MI_x-PAN composite (Figure 2a–d).[68]

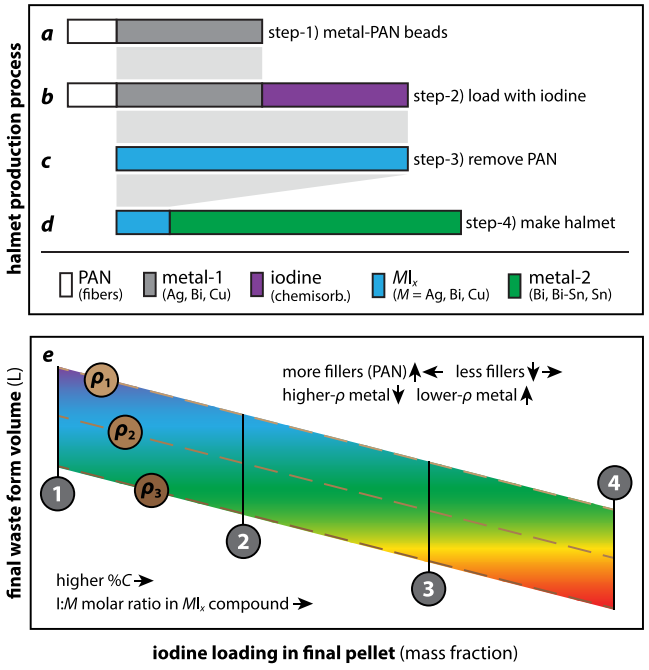

Figure 2. (a–d) Schematic of the proposed method for removing PAN from iodine-loaded metal-PAN composites followed by cermet/halmet synthesis, including (a) making initial metal-PAN beads, (b) loading the metal-PAN beads with iodine, (c) removing the PAN phase, and (d) mixing the MI_x phase with a metal material and making a halmet waste form. Note that a large volume of metal-2 might be used to encapsulate the recovered MI_x compound. (e) Relationships between final waste form volumes and iodine loadings (increasing 1 → 4) with encapsulant metals of different densities (increasing $\rho_1 \rightarrow \rho_3$).

Overall, removing the PAN phase is a benefit for several reasons, but the obvious drawback is that it adds more steps in the process and produces another waste stream containing DMSO. Another point of concern here is that the MI_x compounds could dissolve in the DMSO, and it is possible that some iodine is encapsulated directly in the PAN matrix,[61] which would become mobile upon PAN dissolution within the DMSO. Of course, other solvents might work better than DMSO, so this could be explored. However, it is possible that this process of PAN separation from the MI_x phase could have very large benefits from a volume reduction perspective, so its efficacy is of high importance for advancing these concepts toward implementation. The goal for the final fate of the MI_x phase would be to either (1) isolate it from the PAN and hot press that directly into a waste form or (2) immobilize it in a secondary phase such as a metal to create a halmet-type or cermet-type waste form (Figure 2a–d). Figure 2e provides a graphical representation of the relationships between waste form volume, iodine loading, encapsulant metal density, and the effects of having fillers (e.g., PAN) in the final composite waste form.

2. MATERIALS AND METHODS

2.1. Sample Selection and Synthesis. For the current study, the sample selection included commercial MI_x compounds of AgI (99.999%, Alfa Aesar) and CuI (99.998%, Thermo Scientific), which were used as received. The study also utilized metal-PAN composites including 75Ag-PAN, 75Bi-PAN, and 75Cu-PAN where the amount of metal incorporated into the PAN composites was 75 mass%.[62] For the metal-PAN composites, a brief summary will be provided here but a more detailed account is found elsewhere.[62]

The 75Ag-PAN, 75Bi-PAN, and 75Cu-PAN composite beads were produced by dissolving ∼0.2 g of PAN fibers (×100, 3.3 dtex, 60 mm; Dralon GmbH, Dormagen, Germany) into 3 mL of DMSO (≥99.9%, Sigma-Aldrich) within a glass beaker. After this, ∼0.6 g of metal particles of Ag^0 (≲20 μm, 99.9%), Bi^0 (<44 μm, 99.5%), or Cu^0 (10 μm, 99.9%) were suspended in the mixture; metal particles were procured from Alfa Aesar and used as received. After suspending the metal particles in the PAN–DMSO mixture, this mixture was pipetted into a 5 mL pipet tip sitting ∼5 cm above a chilled (∼1–7 °C) deionized water (DIW) bath being stirred with a magnetic stir bar from underneath. The beads were drawn into the bath and instantly frozen into oblate spheroidal shapes. After dropping the full mixture into the DIW beaker, the DIW was replaced a few times to dilute the DMSO within the bead interiors through passive diffusion. Once the DIW was clear (typically three exchanges totaling ∼400 mL DIW), the beads were removed and put into a vacuum desiccator to dry to constant mass. The resulting beads were ∼2–3 mm in diameter.

2.2. Iodine Loading. Metal-PAN composites were loaded with iodine in static tests at isothermal heat-treatment temperatures (T_{ht}) and heat-treatment times (t_{ht}) shown in Table 2, which were based on expected reaction kinetics from prior work.[62,74] For all experiments, initial sample masses ($m_{s,i}$) were loaded into tared glass sample containers (i.e., either 20 mL glass scintillation vials or 4 mL Qorpak vials, GLC-00980), iodine was loaded into a separate 20 mL scintillation vial and all samples including the iodine were placed inside a 1 L PFA jar (100–1000–01; Savillex; Eden Prairie, Minnesota). Then, the jar was tightly closed with a lid and placed into a vacuum oven (VO914A-1, Thermo Scientific, Lindberg Blue M) for the high precision temperature control, but with the vacuum turned off. Following t_{ht}, the samples were removed from the Savillex jar and placed into a separate oven (3511FSQ, Isotemp, Fisher Scientific; Hampton, New Hampshire) at the same T_{ht} overnight (≈24 h) to desorb any loosely physisorbed iodine.

Table 2. Description of Samples for the Iodine Loading Process Including the Batch ID, Sample Description, Initial Sample Mass ($m_{s,i}$; i.e., before Iodine Loading), Heat-Treatment Temperature (T_{ht}), and Heat-Treatment Time (t_{ht}) in Days[a]

description	sample name	$m_{s,i}$ (g)	T_{ht} (°C)	t_{ht} (days)
Ag^0	$Ag^{(120)}$	0.0292	120	2.0
Bi^0	$Bi^{(120)}$	0.0216	120	2.0
Cu^0	$Cu^{(120)}$	0.0214	120	2.0
75Ag-PAN	75Ag-PAN$^{(130)}$	0.7213	130	4.90
75Bi-PAN	75Bi-PAN$^{(130)}$	0.7290	130	4.90
75Cu-PAN	75Cu-PAN$^{(150)}$	0.1174	150	1.0

[a]The superscripted numbers listed after the sample names denote T_{ht}.

Following iodine loading, final loaded sample masses were collected ($m_{s,f}$) where all mass gained was attributed to iodine,

https://doi.org/10.1021/acsomega.4c03378
ACS Omega 2024, 9, 34661–34674

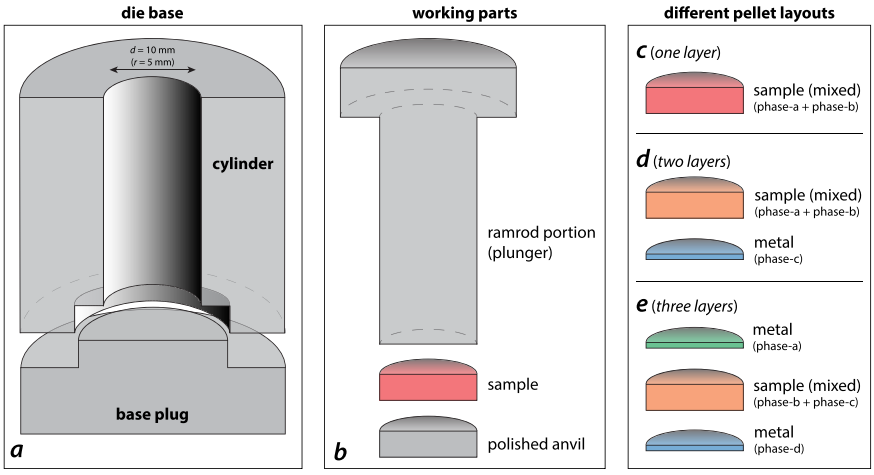

Figure 3. Schematic showing the pelletization process including (a) the pellet die base (cylinder and base plug), (b) additional parts (i.e., the ramrod and anvil) and where the sample fits, and (c–e) different pellet layouts with differing numbers of phases including (c) one layer, (d) two layers, and (e) three layers (sandwich approach). An alternative approach is to use a polished anvil above and below the sample, not just below as shown in the diagram.[58,68] Modified with permission from Evarts et al.[58] Copyright 2024 American Chemical Society.

which disregards the possibility that increased mass could be due to adsorbed and/or absorbed water. Then, several calculations were performed based on these data to assess loading performances. First, the gained mass (m_I) was calculated using eq 1 through a difference between $m_{s,f}$ and $m_{s,i}$. Once m_I was known, the iodine loading (q_e) (eq 2) in milligrams of iodine per gram of starting sorbent was calculated.

$$m_I = m_{s,f} - m_{s,i} \tag{1}$$

$$q_e = {m_I}/{m_{s,i}} (\text{in mg g}^{-1}) \tag{2}$$

Assuming that all iodine was loaded directly onto the metal particles through chemisorption and formed the MI_x compound, the maximum iodine mass possible ($m_{I,max}$) was calculated using eq 3, where mf_{ML} is the mass fractional metal loading in the sorbent (i.e., 1.0 for pure metal particles and 0.75 for the 75 mass% metal-loaded PAN composites), x_I is the molecular weight of iodine, M_I represents the moles of iodine in the MI_x compound (i.e., 1 for AgI, CuI, and BiOI, and 3 for BiI_3), and x_m is the molecular weight of the metal getter in the sorbent. Second, the mass of MI_x formed (m_{MI_x}) was calculated with eq 4, where x_{MI_x} is the molecular weight of the MI_x compound, and the other variables were defined previously. Third, the residual (unreacted) metal mass ($m_{m,r}$) was calculated using eq 5 (similar concept to unreacted getter, $m_{g,r}$ in Figure 1c,d) by difference of the other parameters previously defined with the exception of m_{PAN}, the mass of PAN in the final composite. Finally, the percentage of conversion (%C) of the metal to MI_x was calculated using eq 6.

$$m_{I,max} = {(m_{s,i} \times mf_{ML} \times x_I \times M_I)}/{x_m} \tag{3}$$

$$m_{MI_x} = {(m_I \times x_{MI_x})}/{(x_I \times M_I)} \tag{4}$$

$$m_{m,r} = m_{s,f} - m_{PAN} - m_{MI_x} \tag{5}$$

$$\%C = {m_I}/{m_{I,max}} \times 100 \tag{6}$$

2.3. Making Pellets. The general layout of the pellet die (radius, r = 5 mm) used in this work is shown in Figure 3.[58,68] The pellet-making process varied with several parameters being adjusted over time where some pellets contained separately prepared layers. For multilayer pellets, the anvil (Figure 3b) and previously pressed layers were left in the cylinder (Figure 3a), but the ramrod (Figure 3b) was removed for each subsequent layer being pressed. Pressing pressures differed between the subsequent layers in multilayer pellets. This was done because it is nearly impossible to reinsert a pellet into the cylinder once it has been removed without ruining the edges. For all pellets, a Bi^0 encapsulant was used; this was acquired from American Elements (99.9%, <44 μm).

2.3.1. Making Two-Phase Halmet Pellets. Two-phase pellets were made with commercial MI_x (i.e., AgI and CuI) compounds and Bi^0 encapsulants using the one-layer approach shown in Figure 3c. To make pellets, several physical properties and parameters of each different phase were considered so that pellets of similar dimensions could be produced. The initial cylindrical pellet sizes produced were ~2.5 mm in height (h) with a r of 5 mm and an approximate green pellet volume ($V_{p,g}$) of 0.1964 cm^3, which was calculated using eq 7. The method for calculating the total mass of material needed to achieve this target pellet volume included formulation with eq 8. This was used to determine target masses of phase-a (m_{p-a}; waste-containing material, i.e., ceramic or halide phase) and phase-b (m_{p-b}; encapsulant metal) utilizing the densities of each phase (i.e., ρ_{p-a} and ρ_{p-b}, respectively) to achieve a specific target waste loading in mass % ($WL_{m\%}$) (eq 9). These calculations assumed that all porosity was removed during the pelletization process, which was not the case.

$$V_{p,g} = \pi r^2 h \tag{7}$$

$$V_{p,g} = {m_{p-a}}/{\rho_{p-a}} + {m_{p-b}}/{\rho_{p-b}} = 0.1964 \text{cm}^3 \tag{8}$$

$${m_{p-a}}/{(m_{p-a} + m_{p-b})} \times 100 = WL_{m\%} \tag{9}$$

Once the target masses for phase-a and phase-b were calculated, they were weighed out on an analytical balance

https://doi.org/10.1021/acsomega.4c03378
ACS Omega 2024, 9, 34661−34674

Table 3. Summary of Processing Details for Two-Phase Pellets where Phase-a is the Material to Be Encapsulated and Phase-b Is the Encapsulant Phase (Metal), t_{ht} Is the Heat-Treatment Time, m_p Is the Mass of the Pellet, h_p Is the Pellet Height, $WL_{I,m}$ Is the Expected Mass Loading of Iodine in the Composite Waste Form, and $WL_{MI,v}$ Is the Expected Volumetric Loading of the MI_x Compound in the Final Composite[a]

sample ID	phase-a (mass %)	phase-b (mass %)	t_{ht} (h)	m_p (g)	h_p (mm)	$WL_{I,m}$ (m %)	$WL_{MI,v}$ (vol %)	alt. ID
AgI-halmet	30% AgI	70%Bi^0	22	1.5628	2.58 ± 0.03	16.22	42.5	3c
CuI-halmet	30% CuI	70%Bi^0	20	1.5599	2.59 ± 0.02	19.99	42.5	4a

[a]For both pellets, the balance phase was 70%Bi^0 metal, the target h_p was 2.5 mm, and the value for T_{ht} was 203(±0.5)°C. "Alt. ID." denotes the sample description documented elsewhere for these same samples.[68]

(model ME204E; Mettler Toledo, Columbus, Ohio; ± 0.1 mg), mixed together in a plastic weigh boat (no grinding was performed), and then loaded into the chamber of the steel die. The die was loaded into a uniaxial press (model 3393, Carver, Inc.), and a load of 1000 pounds per square inch (PSI) was applied (based on the Carver pressure dial) for 1 min. After 1 min, the load was released and the pellet was recovered from the die. Using eq 10,[75] the actual applied load pressure (P_A) during this process was calculated where T is the force applied (in metric tons) on the hydraulic cylinder, g is the gravitational acceleration (9.8 m·s^2), and r is the radius of the die (in m). The other option to calculate P_A is to divide the force applied (F_A) by the area of the die face (A_d) to get the applied pressure (P_A), which is also shown in eq 10.

$$P_A = \left.(T\cdot g)\right/(\pi r^2) = \left.F_A\right/A_d \quad (10)$$

Once the pellets were removed from the die, the green pellet masses ($m_{p,g}$) were recorded. Then, the $V_{p,g}$ values were calculated with calipers using two or three different measurements of the diameter and the thickness so that averages could be calculated. This was done because each pellet had some minor irregularities in all dimensions (≈ ± 0.02 mm). After pellets were prepared, they were heat treated under vacuum at 203(±0.5)°C for similar times (Table 3).

2.3.2. Making Three-Phase Polyhalmet Pellet. The calculations for making three-phase pellets (i.e., metal, polymer, and ceramic/halide phases) that included PAN were more complicated. Calculations for these materials assume the following: (1) an even metal loading across all metal-PAN composites, (2) an even iodine loading across all metal-PAN composites, (3) that no mass changes occurred after iodine loading (due to water absorption from the air), and (4) that the PAN does not decompose during the iodine loading process.

Thus, similar equations to those above were used here, but with a few adjustments described below in more detail. After loading the metal-PAN composites with iodine, not all the metal reacted with iodine according to mass changes alone, i.e., comparing measured $m_{s,f}$ and m_I values with expected values. These discrepancies were attributed to residual getter metal mass ($m_{m,r}$) remaining in the beads, and this has to be accounted for when calculating the overall composite volume after iodine loading ($V_{polymet+I}$) using ith phase masses (m_i) and densities (ρ_i) (see eq 11). The three components in this calculation include the PAN matrix (m_{PAN} and ρ_{PAN}), the MI_x (m_{MI_x} and ρ_{MI_x}), and the residual metal ($m_{m,r}$ and $\rho_{m,r}$) where the masses of all components were calculated to achieve the target pellet volume. From these calculations, the mass of iodine waste loading ($WL_{I,m}$) and volumetric waste loading of the MI_x complex ($WL_{MI,v}$) were calculated using eqs 12 and 13, respectively, which includes the volume of the encapsulant metal phase ($V_{m,e}$).

$$V_{polymet+I} = \left.m_{PAN}\right/\rho_{PAN} + \left.m_{MI_x}\right/\rho_{MI_x} + \left.m_{m,r}\right/\rho_{m,r} = 0.1964\,cm^3 \quad (11)$$

$$WL_{I,m} = 100 \times \left.m_I\right/(m_{PAN} + m_{MI_x} + m_{m,r}) \quad (12)$$

$$WL_{MI,v} = \left.V_{MI_x}\right/(V_{polymet+I} + V_{m,e}) \quad (13)$$

In making the three-phase polyhalmet pellet, the approach taken was a three-layer sandwich of the MI_x-PAN precursor [i.e., 75Cu-PAN$^{(150)}$] mixed with 100%Bi^0 as the middle layer (phase-b + phase-c) surrounded by a top layer (phase-a) and bottom layer (phase-d) of 100%Bi^0; this is shown graphically in Figure 3e. This approach was used to provide better encapsulation of the polyhalmet beads with a larger fraction of the "*met*" (i.e., 100%Bi^0) phase for better chemical stability and aid in densification around the compressed 75Cu-PAN$^{(150)}$ beads. While the 100%Bi^0 layers were pulled straight from the as-received chemical bottle, the 75Cu-PAN$^{(150)}$ phase was preground to size reduce through crushing between two plastic weigh boats. This crushing process was used to keep the crushed pellets contained but also aided in transferring them to the die cylinder (Figure 3a). To create this pellet, the initial 100%Bi^0 layer (phase-a) was added, pressed to 1000 PSI (3.1 t), the middle layer was added and pressed to 1500 PSI (∼5 t; phase-b + phase-c), and then the top layer was added and pressed to 1000 PSI (phase-d). Details on the pellet layers are provided in Table 4. Pressing prototypes of multilayer pellets like these could lead to cracking between the different layers during firing, but many of these limitations would be removed

Table 4. Experimental Details for 75Cu-PAN$^{(150)}$ Polyhalmet Pellet Made with Three Layers Including 100% Bi^0 (Phase-a), a Mixture of 75Cu-PAN$^{(150)}$ (Phase-b; See Table 2) and 100%Bi^0 (Phase-c) Followed by Another Layer of 100%Bi^0 (Phase-d)[a]

phase	parameter	value
phase-a (Bi^0)	mass (g)	0.2310
phase-b [75Cu-PAN$^{(150)}$]	mass (g)	0.1889
phase-c (Bi^0)	mass (g)	0.4125
phase-d (Bi^0)	mass (g)	0.2312
pellet properties	h (mm)	2.16
	t_{ht} (h)	20
	$WL_{I,m}$ (mass %)	10.45%
	$WL_{MI,v}$ (vol %)	23.81%

[a]The pellet was fired under vacuum at T_{ht} = 203(±0.5)°C.

https://doi.org/10.1021/acsomega.4c03378
ACS Omega 2024, 9, 34661−34674

if a hot-pressing process were utilized instead of a cold-press-and-sinter approach.

2.4. Removing PAN from MI_x-PAN Composites. Three different samples [i.e., 75Ag-PAN$^{(130)}$, 75Bi-PAN$^{(130)}$, and 75Cu-PAN$^{(150)}$] (see Table 2) were studied for evaluating PAN removal from MI_x-PAN composites, where the general approach was the same. Initial scoping experiments were conducted on whole 75Cu-PAN$^{(150)}$ composite beads that showed slow and limited solubility in DMSO,[68] but subsequent experiments with 75Ag-PAN$^{(130)}$ and 75Bi-PAN$^{(130)}$ utilized composite beads that were crushed between two weigh boats into finer particles to aid in the DMSO accessibility toward the PAN. For the initial dissolution step, the MI_x-PAN composite sample masses ($m_{s,d}$) added to 20 mL glass scintillation vials are shown in Table 5. The volume of DMSO added was 3 mL. Samples were stirred magnetically for several days.

Table 5. Summary of Experiments Performed for PAN Removal Using DMSO after Iodine Loading of PAN Composites[a]

sample ID	75Ag-PAN$^{(130)}$	75Bi-PAN$^{(130)}$	75Cu-PAN$^{(150)}$
Alt. ID	I-3a	I-3b	I-2c
getter	Ag^0	Bi^0	Cu^0
morphology	crushed	crushed	intact
$m_{s,d}$ (g)	0.0317	0.0288	0.067

[a]The ID# denotes the details for the starting sorbent from Table 2, and $m_{s,d}$ is the sample mass for dissolution tests. The "Alt ID" denotes the equivalent sample documented elsewhere.[68] For all samples, 3 mL of DMSO was used (V_{DMSO}).

Following this, the stirring was stopped and the particles were allowed to settle to the bottom of the vials. Samples 75Ag-PAN$^{(130)}$ and 75Bi-PAN$^{(130)}$ were processed further based on having the most promising initial results. The contents of each sample vial (i.e., DMSO mixed with samples, including both soluble and insoluble materials) were transferred to a 50 mL conical centrifuge tube and allowed to settle for an additional 7 days. After this, DMSO was removed from the vial. Then, 4 mL of DIW was added to each vial and mixed with a small magnetic stir bar (from the original glass scintillation vial). The DIW was allowed to sit for 7 days in the container, after which the tubes were loaded into a centrifuge (Sorvall Legend Mach 1.6, Thermo Fisher Scientific) and run for 5 min at 2500 rpms. The liquid was pipetted off the pelletized solids at the bottom, and fresh 4 mL DIW was added and mixed using the stir bar. The centrifugation step was repeated as before, the stir bar was removed, the DIW was discarded, and the centrifuge tubes containing the residual solids were placed inside a glass vacuum desiccator at room temperature to dry to constant mass. The dried samples were analyzed with X-ray diffraction (XRD) described below to determine the crystalline phases present.

2.5. Pellet Characterization. *2.5.1. Images and Optical Microscopy.* Images of pellets were taken with a digital camera. Optical microscopy (OM) was performed on all samples after pellets were mounted in epoxy and vertically cross-sectioned for polishing. The OM was done on a VHX-7000 (Keyence Corporation of America, Itasca, Illinois) using a 20×−200× objective and coaxial lighting.

2.5.2. Scanning Electron Microscopy and Energy-Dispersive X-ray Spectroscopy. All scanning electron microscopy (SEM) was performed on a JSM-7001F field emission gun instrument (JEOL USA, Inc., Peabody, Massachusetts) using probe current 13−15, 15 kV acceleration voltage, and imaging with a backscattered electron (BSE) detector. Energy-dispersive X-ray spectroscopy (EDS) was performed using dual Bruker xFlash 6|60 (Bruker AXS Inc., Madison, Wisconsin) mounted at different angles off the X-ray collection cone.

2.5.3. Electron Probe Microanalysis and Wavelength-Dispersive Spectroscopy. Wavelength-dispersive spectroscopy (WDS) was performed using a JXA-8530F HYPERPROBE electron probe microanalyzer (EPMA) with a field emission gun (JEOL USA, Inc., Peabody, Massachusetts).

2.5.4. Bulk Density (Helium Pycnometry). Bulk densities (ρ_b) of materials were measured using an AccuPyc II 1340 helium pycnometer (Micromeritics instrument Corporation, Norcross, Georgia). To run these experiments, samples were weighed on an analytical balance through difference in mass by taring the sample cup mass before adding sample and then 10 volumetric measurements were measured with the instrument. Using the volumetric data coupled to the mass entry, the instrument software output an average density value with associated standard deviation ($\pm 1\sigma$) values.

2.5.5. X-ray Diffraction. XRD analyses were performed on raw materials (i.e., Bi^0), the unloaded PAN composites, and iodine-loaded PAN composites. XRD analysis was performed using a Bruker D8 Advance (Bruker AXS Inc., Madison, Wisconsin) XRD with Cu Kα emission. The detector used was a LynxEye position-sensitive detector with a collection window of 3° 2θ. Scan parameters were generally within the 10−70° 2θ scan range with a step of 0.02° 2θ and a 1 s dwell at each step.

3. RESULTS AND DISCUSSION

3.1. Iodine Loading Results. The results of the iodine loading experiments with the Ag^0, Bi^0, and Cu^0 particles (without PAN) and the 75Ag-PAN, 75Bi-PAN, and 75Cu-PAN composites are provided in Figure 4, including $m_{s,i}$, m_I, q_e, and %C values; tabulated data are provided in Table S3 (SI). These show clear differences between the performances of the six sorbents in different categories. The cause of lower %C values for Bi^0 and Cu^0 (without PAN) remains unclear, but %C values for the metal-PAN composites were all high.

3.2. Metal-MI_x Halmets. Optical images, SEM micrographs, and EDS dot maps for 70Bi-AgI and 70Bi-CuI are provided in Figure 5. These show the even distribution of AgI and CuI in the Bi^0 matrix phase. Different MI_x particle sizes in the pellets are due to initial particle size distributions in the as-received chemical containers. In some cases, large agglomerates of the MI_x phase are evident in the pellet, which could be minimized if the MI_x phase were ground to a finer particle size prior to pelletization. Bi^0 grain boundaries are evident in both pellets, which could be reduced with higher pressing pressures and higher sintering temperatures. The ineffective particle−particle sintering is also attributed to oxide layer coatings on the Bi^0 particles due to prolonged exposure to air. During the course of this project, it was evident that the Bi^0 started to tarnish; in hindsight, it would be best to store the Bi^0 under vacuum or inert atmosphere when not in use.

SEM-EDS and EPMA-WDS were used to compare the analytical data for the 70Bi-AgI pellet, and this data is presented in Figure 6. The comparison plot shows several key

https://doi.org/10.1021/acsomega.4c03378
ACS Omega 2024, 9, 34661−34674

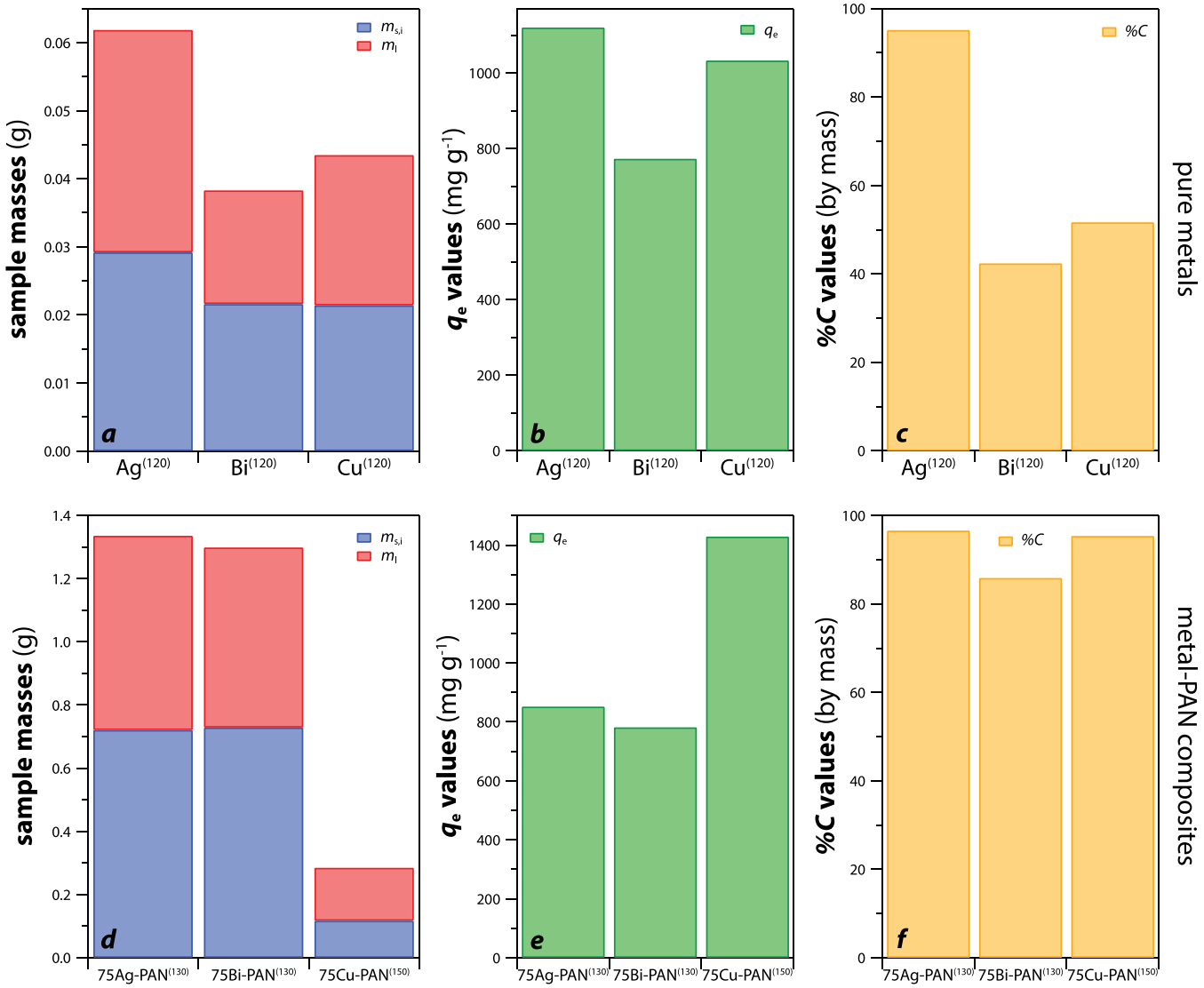

Figure 4. Summary of iodine loading information for (a–c) pure metals and (d–f) metal-PAN composites including (a, d) the $m_{s,i}$ and m_l values, (b, e) q_e values, and (c, f) %*C* values. These data come from Table S3 (SI).

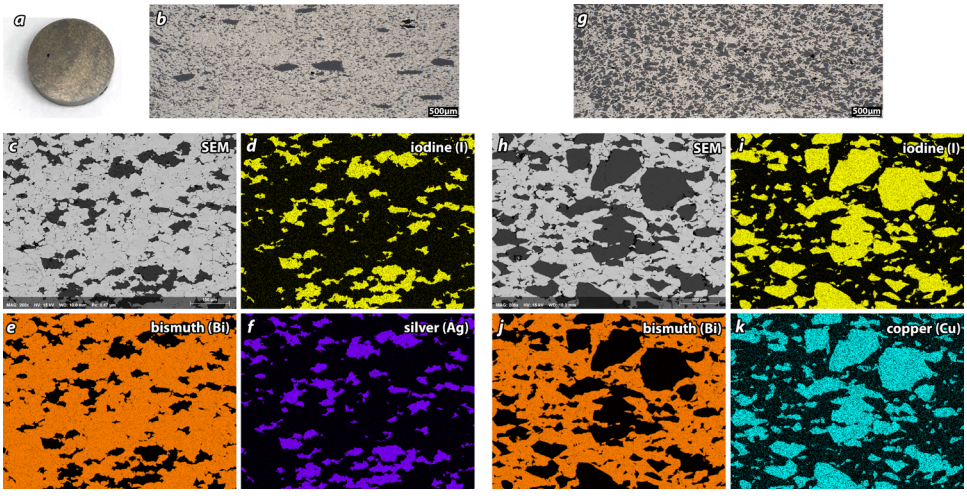

Figure 5. Cross-sectional views of two-phase pellets (a–f) 70Bi-AgI and (g–k) 70Bi-CuI halmets including (a) a picture, (b, g) optical micrographs (50×), (c, h) SEM micrographs, and (d–f, i–k) EDS dot maps.

https://doi.org/10.1021/acsomega.4c03378
ACS Omega 2024, 9, 34661–34674

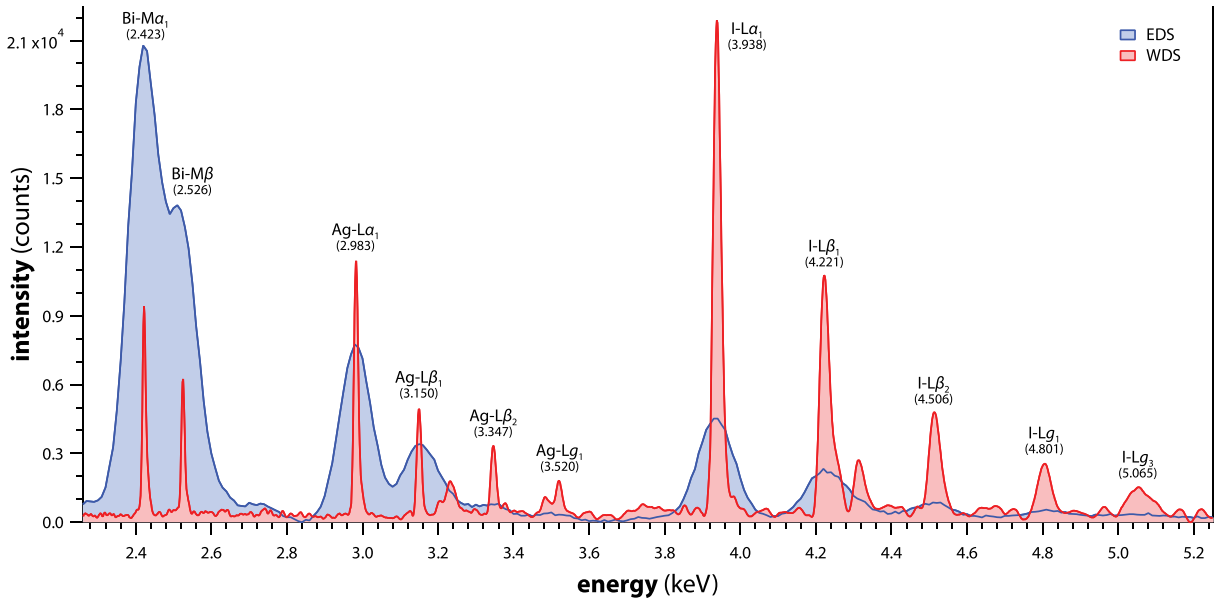

Figure 6. Comparison of EDS and WDS resolution, energy nonlinearities, and peak intensities, for AgI-halmet sample (see Table 3).

differences between these data sets, which include notably higher resolution for WDS over EDS, discontinuous nonlinearities between each data set (i.e., I peaks show up with much lower peak intensities in EDS vs WDS while EDS shows peak heights somewhat proportional to elemental loadings in atomic%), and better peak deconvolution for WDS within many overlapping regions seen in the EDS data set. These data sets provided introductory information for how to chemically measure phases in these types of multiphase pellets. From this work, it was apparent that using this source of Bi^0 would likely result in pellets with low sintering capacity without elevating the temperature. To combat additional Bi^0 oxidation to Bi_2O_3, these pellets and all subsequent pellets were heat treated under vacuum. While these pellets did not fully sinter together with limited particle−particle necking (or none in some regions of the pellet), they demonstrate the concept of halmet production of a low-T_m metal encapsulant (Bi^0) using two different MI_x compounds (AgI and CuI).

3.3. Metal-MI_x-PAN Composite (Polyhalmet). For the Bi^0 + 75Cu-PAN$^{(150)}$ polyhalmet, lighter pressures were used to create the bottom Bi^0 layer, the higher pressure was used to create the Bi^0 + 75Cu-PAN$^{(150)}$ layer, and then the Bi^0 layer was added and the entire pellet was pressed together (i.e., 1000 PSI → 1500 PSI → 1000 PSI, respectively; see Figure 7). Based on the gap between the top Bi^0 layer and the Bi^0 + 75Cu-PAN$^{(150)}$ layer seen in Figure 7b, this "sandwich" approach will require some additional preparations in order to prevent these layers from separating in future pellet production efforts.

Another option for creating these boundary layers would be to use a Bi^0 envelope in a hot-pressing process, e.g., using Bi^0 foil to line a HIP can. Small voids and cracks can be seen throughout the Bi^0 + 75Cu-PAN$^{(150)}$ layer. The carbon map (Figure S1, Supporting Information) from the PAN phase corresponds with the locations of CuI as expected due to the PAN contribution. This concept shows that low firing temperatures used in conjunction with the low-T_m metals (i.e., Bi^0) can be applied for densifying PAN-containing composites. However, more work is needed to fully realize the potential of these types of polyhalmet composite waste forms.

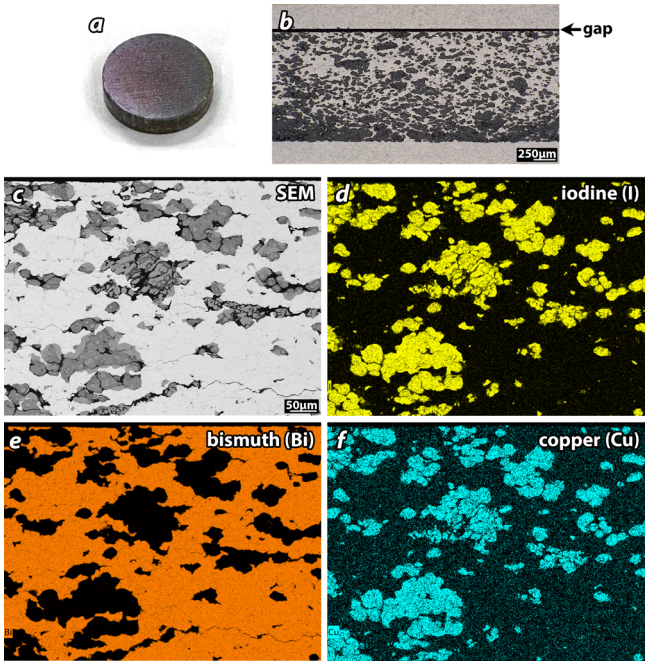

Figure 7. (a) Picture of full polyhalmet pellet after firing, (b) optical micrograph of cross-sectioned view of all layers, (c) SEM, and (d−f) EDS dot maps for the 75Cu-PAN$^{(150)}$ polyhalmet pellet. In (b), the top and bottom layers are Bi^0 and the middle layer is a mixture of Bi^0 + 75Cu-PAN$^{(150)}$. Details for this pellet are provided in Table S1 (SI). The arrow in (b) shows the gap.

Obvious improvements needed include higher pressing pressures, more reactive metal surfaces (i.e., using less oxidized Bi^0, in this case), higher MI_x loadings to improve overall waste loading, and demonstration at higher-volume scales. Improving these aspects of the process will provide the ability to achieve higher overall iodine loadings with smaller overall waste form volumes (bottom right corner of Figure 2e). Another way to help achieve this target location in Figure 2e is by removing the PAN matrix, which is discussed in the next section.

https://doi.org/10.1021/acsomega.4c03378
ACS Omega 2024, 9, 34661−34674

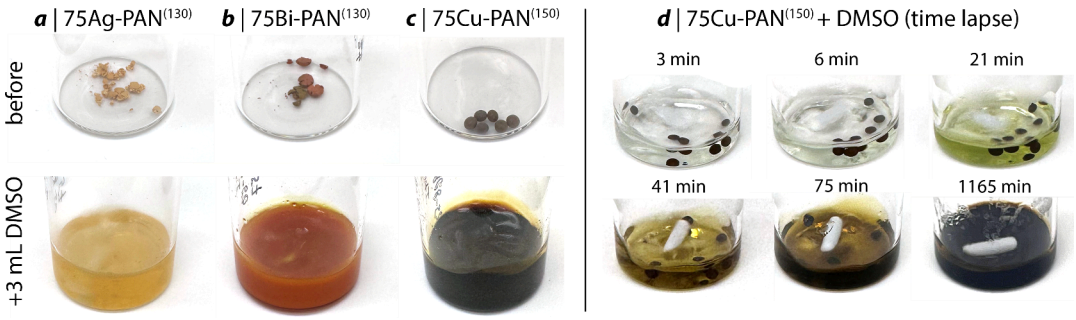

Figure 8. Pictures of (a) 75Ag-PAN$^{(130)}$, (b) 75Bi-PAN$^{(130)}$, and (c) 75Cu-PAN$^{(150)}$ (top) pellets before dissolution in DMSO and (bottom) in 3 mL of DMSO within 20 mL glass vials. The elapsed times since DMSO was added are ≈20 min for (a) and (b) and 5 days for (c). (d) Time-lapse pictures for 75Cu-PAN$^{(150)}$ dissolution in DMSO over 1165 min.

3.4. Removing PAN from MI_x-PAN Composites. Based on the complex microstructures present in the PAN-containing pellet (i.e., Bi^0 + 75Cu-PAN$^{(150)}$) and complications with leaving the PAN phase in the final composite (including the addition of unwanted volume and low-ρ contribution), options to remove the PAN phase from iodine-loaded PAN composites (prior to pelletization) were explored. Pictures of small-scale experiments to assess feasibility of this process are summarized in Figure 8a–c for 75Ag-PAN$^{(130)}$, 75Bi-PAN$^{(130)}$, and 75Cu-PAN$^{(150)}$.

The initial test was conducted with 75Cu-PAN$^{(150)}$ using intact beads, but the dissolution rate was very slow (Figure 8c,d). For the 75Cu-PAN$^{(150)}$ test, a time lapse of solution appearance is provided in Figure 8d; the initial solution color was light yellow, and it gradually turned darker until it was completely opaque after 1165 min. After that experiment, crushed beads were used for the next set of samples with 75Ag-PAN$^{(130)}$ and 75Bi-PAN$^{(130)}$ to see if this sped up the dissolution rate of the PAN phase. For 75Ag-PAN$^{(130)}$ and 75Bi-PAN$^{(130)}$, the dissolution behaviors were very different from one another. The 75Ag-PAN$^{(130)}$ sample appeared to dissolve the PAN fairly rapidly where a fine particulate product was found on the bottom of the container and the solution turned a light yellowish orange color (Figure 8a). For 75Bi-PAN$^{(130)}$, the solution immediately started to turn red and no evidence of residual particulates was observed after approximately 5–10 min (Figure 8b). The 75Ag-PAN$^{(130)}$ and 75Bi-PAN$^{(130)}$ samples showed the most promise based on the solids volume reductions and visible solid size reductions.

After letting the vials sit, 75Ag-PAN$^{(130)}$ showed a layer of particles on the bottom of the vial. For 75Bi-PAN$^{(130)}$, the DIW was notably orange suggesting either some dissolution or fine particles that remained suspended after the centrifugation process.

The results of centrifugation and pelletization of the recovered products at the bottom of the 50 mL centrifuge tubes are shown on the right side of each image set in Figure 9. The dried products were analyzed with XRD and found to be phase-pure AgI (i.e., a mixture of hexagonal β-AgI called iodargyrite and cubic γ-AgI called miersite) for 75Ag-PAN$^{(130)}$ and phase-pure BiOI for 75Bi-PAN$^{(130)}$ (see Figure S2, Supporting Information). This mixture of hexagonal β-AgI and cubic γ-AgI being present in iodine-loaded AgI compounds has been documented many times in similar studies.[28,62,74,76−78]

The original sample masses used ($m_{s,d}$), and the sample masses recovered ($MI_{x,r}$) from these experiments are provided in Table 6. The calculated MI_x present in the original materials

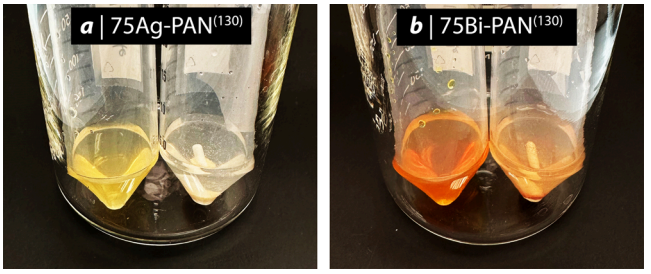

Figure 9. Pictures showing the DMSO dissolution phase in 50 mL centrifuge tubes for (a) 75Ag-PAN$^{(130)}$ and (b) 75Bi-PAN$^{(130)}$ samples. For each set, the tube on the left is the initial DMSO solution pipetted off the residual particles at the bottom, and the tube on the right is the recovered particle pellet with fresh DIW added. The white stir bars can be seen in the tubes.

Table 6. Summary of Initial Sample Masses ($m_{s,d}$), Initial MI_x Masses Present in the Iodine-Loaded Composites ($MI_{x,i}$), Recovered Masses ($MI_{x,r}$), and Mass Recoveries (R%) from DMSO-PAN Dissolution Tests

sample	$m_{s,d}$	$MI_{x,i}$	$MI_{x,r}$	R%
75Ag-PAN$^{(130)}$	0.0317	0.0280	0.0217	77.4%
75Bi-PAN$^{(130)}$	0.0288	0.0205	0.0071	34.7%

($MI_{x,i}$) and the recovered mass percentages (R%), calculated using eq 14, are also provided in Table 6. These calculations were performed assuming the entire recovered product, which consisted of MI_x compounds based on the XRD data provided in Figure S2 (SI). The R% values show that the recoveries were not perfect. A portion of the missing masses are likely due to MI_x dissolution in the DMSO (and possibly DIW over prolonged exposure times) based on the color of the residual rinse solution (see left centrifuge tubes in both Figure 9a and b) and/or fine suspended particles (coloring the solutions). Additionally, some iodine could have been lost between the iodine-loading process to produce the 75Bi-PAN$^{(130)}$ sample where BiI_3 and BiOI were observed with XRD, but where only BiOI was observed in the recovered product after DMSO dissolution tests. This makes calculating the actual recovery difficult for 75Bi-PAN$^{(130)}$. Either way, the AgI phase appeared to be more stable in the DMSO than BiI_3/BiOI based on the observations provided above. It is also likely that the PAN dissolution step would have different results if different organic solvents were used in place of DMSO.[79] Additional studies looking at PAN dissolution in iodine-loaded PAN composites

https://doi.org/10.1021/acsomega.4c03378
ACS Omega 2024, 9, 34661−34674

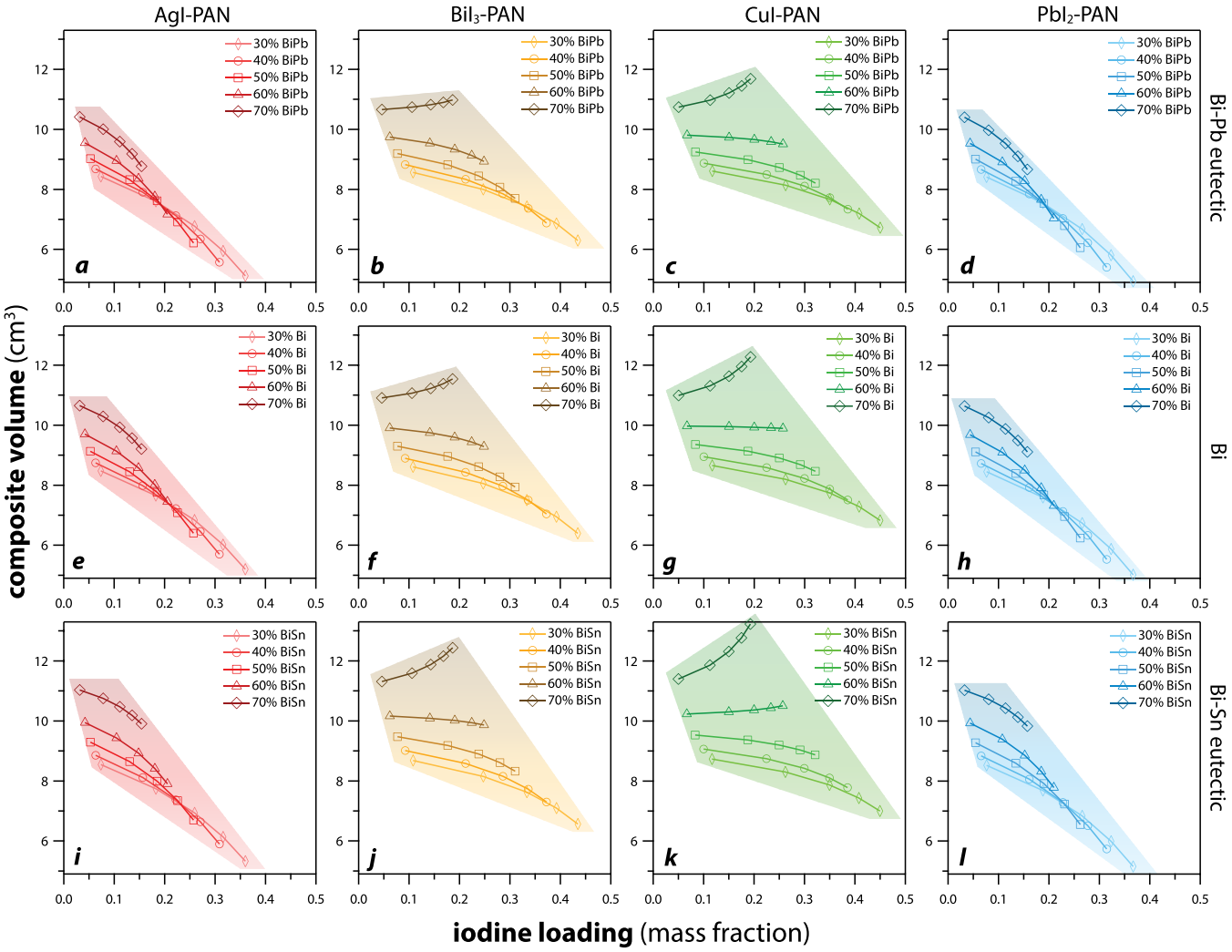

Figure 10. Summary of composite volume (cm^3) vs iodine loading (mass fraction) starting from a fixed metal-PAN composite mass of 10 g, including (a, e, i) AgI-PAN, (b, f, j) BiI_3−PAN, (c, g, k) CuI-PAN, and (d, h, l) PbI_2-PAN embedded in different masses (30−70 mass% of composite) of varying encapsulants, i.e., (a−d) Bi−Sn eutectic (58Bi-42Sn), (e−h) Bi, and (i−l) Bi−Pb eutectic (55.5Bi-44.5Pb). For each data set, five separate composites are included ranging from 10 to 90 mass% active getter (i.e., Ag^0, Bi^0, Cu^0, or Pb^0) in PAN (90−10 mass%), from left to right, respectively. Data were calculated assuming full metal reaction to form MI_x compounds, and all porosity was removed during composite production. This figure is an expansion of Figure 2e. All plots are shown on the same *x*-axis and *y*-axis scales.

could include solution analyses to trace iodine partitioning (mass balance) across the different steps.

$$R\% = 100^{*}MI_{x,r} \Big/ MI_{x,i} \tag{14}$$

3.5. Additional Comparisons and Future Considerations. Considering all the information presented thus far, the next steps in the development process for these types of composite waste forms are discussed within this section. As shown in Table 1, several MI_x compounds could be considered within the context of this framework. While AgI has been studied extensively as a long-term disposal option for radioiodine,[80] other potential MI_x compounds, including BiI_3,[35,62,81,82] BiOI,[35,81,82] CuI,[62,83] and PbI_2,[19] have not been studied as extensively but warrant more attention. These nonstandard MI_x compounds were included in this work as concepts to explore in future studies. Other considerations for the getter metal selection include the cost of the metal and the metal sensitivity to oxidation under expected operating conditions. In this context, Ag^0 is the most expensive, but also the most widely implemented, getter for $I_{2(g)}$ capture, and it is the least sensitive to oxidation being that it is a precious (noble) metal. When considering long-term disposal options for radioiodine, some material properties that need to be evaluated for the prospective MI_x compound are the chemical durability, iodine loading in the compound (WL_I), the thermal stability of the compound (i.e., T_m and T_b), reactivity of the compound, and the ρ_b of the compound.[74,84]

Figure 10 provides a comparison of the WL_I and composite waste form volume for different MI_x compounds encapsulated in different metal matrices (i.e., 55.5Bi-44.5Pb eutectic > Bi^0 > 58Bi-42Sn eutectic). Figure 10 was produced to show the wide variations in storage volumes (waste form volume per mass of immobilized iodine)[59] when these variables fluctuate. The overall composite volumes vary extensively across different MI_x compounds, different metal encapsulants, and different encapsulant loadings. In looking at these data, parameter selections for minimizing overall composite volume and maximizing the iodine loading require several conditions to be met. These include the following: the specific MI_x should be

https://doi.org/10.1021/acsomega.4c03378
ACS Omega 2024, 9, 34661−34674

chosen where WL_I is maximized (e.g., CuI > BiI_3 > PbI_2 > AgI > BiOI; see Table 1), the encapsulant metal should be selected so that it has a high ρ_b (e.g., 55.5Bi-44.5Pb eutectic > Bi^0 > 58Bi-42Sn eutectic > Sn^0; see Table S2, Supporting Information), the metal encapsulant loading should be minimized, and the fillers (e.g., PAN, support structure) should be minimized. The total metal volume required to fully encapsulate the MI_x compound will be higher if the MI_x compound is present within a separate support (e.g., zeolite, aerogel, xerogel) where the support will add volume to the overall waste stream requiring encapsulation. All these aspects need to be simultaneously considered with the overall composite properties in mind, where the chemical durability of the final composite is of utmost importance.

If the polymer phase is left within the final composite, the heat-treatment temperature for the final consolidation step would have to be minimized to below the T_d of the polymer phase. This is why the encapsulant metals with low-T_m values (see Table S2, Supporting Information) ranging 124−271 °C (i.e., 55.5Bi-44.5Pb < 58Bi-42Sn < Sn^0 < Bi^0) were chosen for experiments and conceptual analyses within this study. These metals were also selected and considered based on favorable reactions with $I_{2(g)}$ to form MI_x compounds in the event the iodine was released from the original MI_x compound. However, SnI_4 has since been determined to be less of an effective iodine compound than the other candidates.[73] If the polymer phase was removed prior to the final consolidation step, then higher-T_m encapsulant metals that have better mechanical properties and higher chemical durabilities could be explored, e.g., Cu^0.

Revisiting the concept of an MI_x compound embedded within a passive substrate (that is not a polymer phase), an example of this was demonstrated where iodine-loaded silver faujasite (IONEX Ag-400) was embedded in a Bi^0 matrix (see Figures S3 and S4, Supporting Information) using the same sandwich approach used for the Bi^0/75Cu-PAN$^{(150)}$ polyhalmet (see Figures 3e and7). This particular pellet, which is referred to as the AgIX$^{(150)}$-Bi^0 halcermet, had the same issue of delamination between the pellet layers (Figure S3a,b, Supporting Information) as was observed for the polyhalmet sample (see Figure 7b). In this case, the residual aluminosilicate phase is the ceramic (cer) phase.

It is worth noting that PAN-based composite sorbents show promise regarding radiation stability.[79] Studies by Riley et al.[65] and Robinson et al.[85] demonstrated that PAN composites are stable after γ-ray irradiation exposures up to 1 MGy.

Considering the possibilities of multiphase composites discussed above and summarized in Figure 1, a wide range of potential combinations can be realized using the cold-press-and sinter process. However, to fully realize the potential of these types of composites, hot pressing is likely needed to minimize open porosity (e.g., gaps between grain boundary), maximize particle−particle interactions, and minimize overall composite volumes. Hot pressing (e.g., HIP, SPS) has the added benefit of being done under an inert atmosphere or under vacuum to significantly limit metal-oxide layer formation that hinders effective sintering. A recent review[58] discusses the key properties that need to be considered when optimizing a cermet composite for different phase compositions, which include thermal conductivity, chemical durability, and waste loading so these should be at the forefront of considerations for future studies.

To date, these types of composite forms containing polymer phases have not been demonstrated at a large scale but could be scaled up. Using the high metal loadings achieved in the PAN composites for gettering iodine as well as minimal metal encapsulant phase, the achievable waste loadings provide substantial improvements over traditional approaches with zeolites.[21,47] Also, the added chemical barrier layer of the metal encapsulant has the potential to improve the chemical durability of the composite form over waste forms produced with other types of encapsulants (e.g., glass, ceramic).

4. SUMMARY AND CONCLUSIONS

The work described within this paper could help build the foundation for a new type of composite waste form that contains a salt waste phase, a polymer phase, and an encapsulant metal phase, which is referred to here as a polyhalmet. The concepts discussed herein include low-T_m metal encapsulants that were chosen due to the temperature limitations (low T_d) of the target polymer phase (PAN). To understand the halide salt interactions with a low-T_m encapsulant metal (i.e., Bi^0), halmets were produced using a 1-layer approach, and studied including AgI+Bi^0 and CuI+Bi^0. Both halmet composites resulted in dense monolithic waste forms with low porosities. The polyhalmet composite [i.e., 75Cu-PAN$^{(150)}$-Bi^0] and halcermet composite [i.e., AgIX$^{(150)}$-Bi^0] waste forms showed effective consolidation with some residual porosity due to compressibility limitations with the way the pellets were produced using the three-layer sandwich approach.

This conceptual framework was expanded upon by considering different MI_x (i.e., AgI, BiI_3, BiOI, PbI_2) and metal encapsulant options (i.e., 55.5Bi-44.5Pb eutectic, 58Bi-42Sn eutectic) that might work for this type of composite production methodology due to favorable metal−iodine reactions with these metals in the event the iodine is released from the primary MI_x present after sorbent loading. This is an added benefit of the selection of the encapsulant metals, where it can act as a secondary getter (barrier) for any iodine released from the primary sorbent.

If a polymer phase is present in the original sorbent, options were provided for removing the polymer phase from that sorbent to reduce the overall waste volume in the final waste form. Removing the polymer phase also improves the thermal stability for waste form production step but will add additional processing steps and another waste stream.

Radioiodine stability is very important in the final form, and this requires several conditions to be met. Some of the most important aspects of the selected MI_x compound for disposal include the chemical durability, iodine loading in the compound (WL_I), the thermal stability of the compound (i.e., T_m and T_b), reactivity of the compound, and the ρ_b of the compound. Options for maximizing iodine loading in composite sorbents can be summarized as the following: the selection of MI_x should be done where WL_I is maximized, the encapsulant metal should be selected so that it has a high ρ_b, the metal encapsulant loading should be minimized, and the fillers should be minimized. The most effective method for producing composites like these would be a hot-pressing process such as HIP or SPS, which would help close open porosity and reduce the effects of oxidation on the metal encapsulant. Also, using HIP would fully encapsulate the MI_x compound and aid in protection toward release to the environment. Lastly, the desired outcome of this process is

https://doi.org/10.1021/acsomega.4c03378
ACS Omega 2024, 9, 34661−34674

to find a suitable long-term storage option for radioiodine with the lowest possible storage volume (lowest waste form volume per mass of immobilized iodine) while maintaining the other desired parameters mentioned above.

The primary reason for pursuing these polymer-containing composites is because PAN-containing sorbents show high promise for iodine capture. Thus, the fate of iodine-loaded PAN composites requires technology development before they could be considered a somewhat feasible alternative to porous, passive inorganic scaffolds (e.g., zeolites, aerogels, xerogels) for holding active iodine getters in place during the capture process. This paper aimed to fill in some of the technology development gaps for packaging PAN composite technologies into waste forms for disposal.

■ ASSOCIATED CONTENT

Supporting Information

The Supporting Information is available free of charge at https://pubs.acs.org/doi/10.1021/acsomega.4c03378.

Information on pellet properties, additional SEM-EDS data, additional XRD data, and properties of metal encapsulants (PDF)

■ AUTHOR INFORMATION

Corresponding Author

Brian J. Riley − *Pacific Northwest National Laboratory, Richland, Washington 99354, United States;* orcid.org/0000-0002-7745-6730; Email: brian.riley@pnnl.gov

Authors

Nathan L. Canfield − *Pacific Northwest National Laboratory, Richland, Washington 99354, United States*

Saehwa Chong − *Pacific Northwest National Laboratory, Richland, Washington 99354, United States;* orcid.org/0000-0002-4722-0022

Jarrod V. Crum − *Pacific Northwest National Laboratory, Richland, Washington 99354, United States*

Complete contact information is available at: https://pubs.acs.org/10.1021/acsomega.4c03378

Notes

The authors declare no competing financial interest.

■ ACKNOWLEDGMENTS

This research was supported by the Strategic Investments, under the Laboratory Directed Research and Development (LDRD) Program at Pacific Northwest National Laboratory (PNNL). PNNL is a multiprogram national laboratory operated for the U.S. Department of Energy (DOE) by Battelle Memorial Institute under Contract No. DE-AC05-76RL01830. Authors thank Alexander Kendall, Matt O'Neill, and Barbara Beller for project support and Jared Oshiro for experimental support.

■ REFERENCES

(1) Usman, M.; Radulescu, M. Examining the role of nuclear and renewable energy in reducing carbon footprint: Does the role of technological innovation really create some difference? *Sci. Total Environ.* **2022**, *841*, No. 156662.

(2) Soelberg, N. R.; Garn, T. G.; Greenhalgh, M. R.; Law, J. D.; Jubin, R.; Strachan, D. M.; Thallapally, P. K. Radioactive Iodine and Krypton Control for Nuclear Fuel Reprocessing Facilities. *Sci. Technology Nucl. Installations* **2013**, *2013*, 1.

(3) Zhang, S.; Du, J.; Xu, C.; Schwehr, K. A.; Ho, Y. F.; Li, H. P.; Roberts, K. A.; Kaplan, D. I.; Brinkmeyer, R.; Yeager, C. M.; et al. Concentration-Dependent Mobility, Retardation, and Speciation of Iodine in Surface Sediment from the Savannah River Site. *Environ. Sci. Technol.* **2011**, *45*, 5543.

(4) Tokonami, S.; Hosoda, M.; Akiba, S.; Sorimachi, A.; Kashiwakura, I.; Balonov, M. Thyroid doses for evacuees from the Fukushima nuclear accident. *Sci. Rep.* **2012**, *2*, 507.

(5) Zablotska, L. B.; Ron, E.; Rozhko, A. V.; Hatch, M.; Polyanskaya, O. N.; Brenner, A. V.; Lubin, J.; Romanov, G. N.; McConnell, R. J.; O'Kane, P.; et al. Thyroid cancer risk in Belarus among children and adolescents exposed to radioiodine after the Chornobyl accident. *Br. J. Cancer* **2011**, *104*, 181.

(6) Greaney, A. T.; Ngelale, R. O.; Bruffey, S. H.; Martin, L. R. Abatement of radioiodine in aqueous reprocessing off-gas. *Front. Chem.* **2023**, *10*, No. 1078668.

(7) Riley, B. J.; Vienna, J. D.; Strachan, D. M.; McCloy, J. S.; Jerden, J. L., Jr Materials and processes for the effective capture and immobilization of radioiodine: A review. *J. Nucl. Mater.* **2016**, *470*, 307.

(8) Collard, G. E. R.; Hennart, D.; Van Dooren, J.; Goosens, W. R. A. Iodine trapping and conditioning in the Mercurex process. In *Proceedings of the 16th DOE Nuclear Air and Cleaning Conference*, San Diego, CA 1980 (pp. 20-23).

(9) Trevorrow, L. E.; Vandegrift, G. F.; Kolba, V. M.; Steindler, M. J. *Compatibility of Technologies with regulations in the waste management of H-3, I-129, C-14, and Kr-85. Part I. Initial information base*, ANL-83−57, Argonne National Laboratory: Argonne, IL, 1983.

(10) Mailen, J. C.; Horner, D. E. Removal of radioiodine from gas streams by electrolytic scrubbing. *Nucl. Technol.* **1976**, *30*, 317.

(11) Horner, D. E.; Mailen, J. C.; Posey, F. A. "Electrolytic trapping of iodine from process gas streams," United States patent application#: 4004993, 1977.

(12) Holladay, D. W. *A literature survey: Methods for the removal of iodine species from off-gases and liquid waste streams of nuclear power and nuclear fuel reprocessing plants, with emphasis on solid sorbents*, ORNL/TM-6350, Oak Ridge National Laboratory: Oak Ridge, TN, 1979.

(13) Stromatt, R. *Removal of Radioiodine from PUREX Off-Gases with Nitric Acid and Nitric Acid-Mercuric Nitrate Solutions*, USAEC HW-55735, Hanford Atomic Products Operation: Richland, WA, 1958.

(14) Trowbridge, L. D.; Toth, L. M.; Collins, E. D. *Molten Hydroxide Trapping Process for Radioiodine*, ORNL/TM-2002/247, Oak Ridge National Laboratory: Oak Ridge, TN, 2003.

(15) Riley, B. J.; McFarlane, J.; DelCul, G. D.; Vienna, J. D.; Contescu, C. I.; Forsberg, C. W. Molten salt reactor waste and effluent management strategies: A review. *Nucl. Eng. Des.* **2019**, *345*, 94.

(16) Maeck, W. J.; Pence, D. T. Application of the metal zeolites to radioactive air cleaning problems. In *Proc. 11th AEC Air Cleaning Conference*, CONF-700816. Vol. 2.

(17) Pence, D. T.; Duce, F. A.; Maeck, W. J. Study of the adsorption properties of metal zeolites for airborne iodine species. In *Proc. 11th AEC Air Cleaning Conference*, CONF 700816. 1970.

(18) Pence, D. T.; Duce, F. A.; Maeck, W. J. Developments in the removal of airborne iodine species with metal substituted zeolites. In *Proc. 12th AEC Air Cleaning Conference*, CONF 720823. 1972.

(19) Thomas, T. R.; Murphy, L. P.; Staples, B. A.; Nichols, J. T. *Airborne elemental iodine loading capacities of metal zeolites and a method for recycling silver zeolite*, ICP-1119, Idaho National Laboratory: Idaho Falls, ID, 1977.

(20) Chapman, K. W.; Chupas, P. J.; Nenoff, T. M. Radioactive Iodine Capture in Silver-Containing Mordenites through Nanoscale Silver Iodide Formation. *J. Am. Chem. Soc.* **2010**, *132*, 8897.

(21) Bruffey, S. H.; Jordan, J. A.; Jubin, R. T.; Parks, M. L.; Watkins, T. R. *Hot Isostatic Pressing of Engineered Forms of I-AgZ*, NTRD-MRWFD-2017−000412, ORNL/SR-2017/707, Oak Ridge National Laboratory: Oak Ridge, TN, 2017.

(22) Modolo, G. O. R. Separation of iodine from AC 6120 adsorber material for transmutation. In *Proc. Global 1995 - ANS International Conference on Evaluation of Emerging Nuclear Fuel Cycle Systems*. CONF-950919.
(23) Yadav, A.; Chong, S.; Riley, B. J.; McCloy, J. S.; Goel, A. Iodine capture by Ag-loaded solid sorbents followed by Ag recycling and iodine immobilization: An end-to-end process. *Ind. Eng. Chem. Res.* **2023**, *62*, 3635.
(24) Mineo, H.; Gotoh, M.; Iizuka, M.; Fujisaki, S.; Hagiya, H.; Uchiyama, G. Applicability of a model predicting iodine-129 profile in a silver nitrate silica-gel column for dissolver off-gas treatment of fuel reprocessing. *Sep. Sci. Technol.* **2003**, *38*, 1981.
(25) Mineo, H.; Gotoh, M.; Iizuka, M.; Fujisaki, S.; Uchiyama, G. A Simple Model Predicting Iodine Profile in a Packed Bed of Silica-Gel Impregnated with Silver Nitrate. *J. Nucl. Sci. Technol.* **2002**, *39*, 241.
(26) Tanabe, H.; Sakuragi, T.; Yamaguchi, K.; Sato, T.; Owada, H. Development of new waste forms to immobilize iodine-129 released from a spent fuel reprocessing plant. *Adv. Sci. Technol.* **2010**, *73*, 158.
(27) Riley, B. J.; Chong, S.; Zhao, M.; Lian, J. Densification and Immobilization of AgI-Containing Iodine Waste Forms Using Spark Plasma Sintering. *Ind. Eng. Chem. Res.* **2023**, *62*, 8779.
(28) Riley, B. J.; Chong, S.; Schmid, J.; Marcial, J.; Nienhuis, E. T.; Bera, M. K.; Lee, S.; Canfield, N. L.; Kim, S.; Derewinski, M. A.; et al. Role of zeolite structural properties toward iodine capture: A head-to-head evaluation of framework type and chemical composition. *ACS Appl. Mater. Interfaces* **2022**, *14*, 18439.
(29) Chong, S.; Riley, B. J.; Baskaran, K.; Sullivan, S.; El Khoury, L. G.; Carlson, K.; Asmussen, R. M.; Fountain, M. S. Static iodine loading comparisons between activated carbon, zeolite, alumina, aerogel, and xerogel sorbents. *New J. Chem.* **2024**, *48*, 9880.
(30) Cordova, E. A.; Garayburu-Caruso, V.; Pearce, C. I.; Cantrell, K. J.; Morad, J. W.; Gillispie, E. C.; Riley, B. J.; Colon, F. C.; Levitskaia, T. G.; Saslow, S. A.; et al. Hybrid sorbents for ^{129}I capture from contaminated groundwater. *ACS Appl. Mater. Interfaces* **2020**, *12*, 26113.
(31) Tesfay Reda, A.; Pan, M.; Zhang, D.; Xu, X. Bismuth-based materials for iodine capture and storage: A review. *J. Environ. Chem. Eng.* **2021**, *9*, No. 105279.
(32) Tian, Z.; Chee, T.-S.; Zhu, L.; Duan, T.; Zhang, X.; Lei, L.; Xiao, C. Comprehensive comparison of bismuth and silver functionalized nickel foam composites in capturing radioactive gaseous iodine. *J. Haz. Mater.* **2021**, *417*, No. 125978.
(33) Hao, Y.; Tian, Z.; Liu, C.; Xiao, C. Recent advances in the removal of radioactive Iodine by bismuth-based materials. *Front. Chem.* **2023**, *11*, No. 1122484.
(34) Baskaran, K.; Ali, M.; Riley, B. J.; Zharov, I.; Carlson, K. Evaluating the physisorption and chemisorption of iodine on bismuth-functionalized carbon foams. *ACS Mater. Lett.* **2022**, *4*, 1780.
(35) Baskaran, K.; Elliott, C.; Ali, M.; Moon, J.; Beland, J.; Cohrs, D.; Chong, S.; Riley, B. J.; Chidambaram, D.; Carlson, K. Effects of NO_2 aging on bismuth nanoparticles and bismuth-loaded silica xerogels for iodine capture. *J. Haz. Mater.* **2023**, *446*, No. 130644.
(36) Metalidi, M. M.; Beznosyuk, V. I.; Kalinin, N. N.; Kolyadin, A. B.; Fedorov, Y. S. Treatment of gas-air flows to remove radioiodine using metallic copper. *Radiochem.* **2009**, *51*, 409.
(37) Zhou, J.; Chen, Q.; Li, T.; Lan, T.; Bai, P.; Liu, F.; Yuan, Z.; Zheng, W.; Yan, W.; Yan, T. Porous Copper-Loaded Zeolites for High-Efficiency Capture of Iodine from Spent Fuel Reprocessing Off-Gas. *Inorg. Chem.* **2022**, *61*, 7746.
(38) Riley, B. J.; Chong, S.; Olszta, M. J.; Peterson, J. A. Evaluation of getter metals in Na-Al-Si-O aerogels and xerogels for the capture of iodine gas. *ACS Appl. Mater. Interfaces* **2020**, *12*, 19682.
(39) Riley, B. J.; Chong, S.; Canfield, N. L. Synthesis of and iodine capture with MS_x (Ag_2S, Bi_2S_3, Cu_2S)−polyacrylonitrile composites. *New J. Chem.* **2024**, *48*, 3352.
(40) McCloy, J. S.; Stone-Weiss, N.; Bollinger, D. L. Caustic scrubber waste converted to aluminosilicates: Structures determined by nuclear magnetic resonance. *MRS Adv.* **2023**, *8*, 261.
(41) Vance, E. R.; Davis, J.; Olufson, K.; Chironi, I.; Karatchevtseva, I.; Farnan, I. Candidate waste forms for immobilisation of waste chloride salt from pyroprocessing of spent nuclear fuel. *J. Nucl. Mater.* **2012**, *420*, 396.
(42) Cao, C.; Chong, S.; Thirion, L.; Mauro, J. C.; McCloy, J. S.; Goel, A. Wet chemical synthesis of apatite-based waste forms − A novel room temperature method for the immobilization of radioactive iodine. *J. Mater. Chem. A* **2017**, *5*, 14331.
(43) Audubert, F.; Carpena, J.; Lacout, J.-L. "Method of packaging radioactive iodine, in particular iodine 129, using apatite as the confinement matrix," France patent application#: EP0744074 B1, 1998.
(44) Audubert, F.; Lartigue, J. Iodine immobilization in apatites. In*Proc. Atalante*. p P4.13-1.
(45) Nam, J.; Chong, S.; Riley, B. J.; McCloy, J. S. Iodosodalite Waste Forms from Low-Temperature Aqueous Process. *MRS Adv.* **2018**, *3*, 1093.
(46) Chong, S.; Peterson, J.; Nam, J.; Riley, B.; McCloy, J. Synthesis and characterization of iodosodalite. *J. Am. Ceram. Soc.* **2017**, *100*, 2273.
(47) Bruffey, S. H.; Jubin, R. T.; Jordan, J. A. *Fundamental Aspects of Zeolite Waste Form Production by Hot Isostatic Pressing*, FCRD-MRWFD-2016−000267, ORNL/SR-2016/759, Oak Ridge National Laboratory: Oak Ridge, TN, 2016.
(48) Jubin, R. T.; Bruffey, S. H.; Patton, K. K. *Expanded Analysis of Hot Isostatic Pressed Iodine-Loaded Silver-Exchanged Mordenite*, FCRD-SWF-2014−000278; ORNL/LTR-2014/476, Oak Ridge National Laboratory Oak Ridge: TN, 2014.
(49) Bruffey, S. H.; Jubin, R. T. *Preparation of Four Large Format Hot Isostatically Pressed I-AgZ. Waste Form Samples for Performance Testing*, NTRD-MRWFD-2018−000198; ORNL/SPR-2018/1026, Oak Ridge National Laboratory: Oak Ridge, TN, 2018.
(50) Bruffey, S. H.; Jubin, R. T. *Recommend HIP Conditions for AgZ*, FCRD-MRWFD-2015−000423, ORNL/SPR-2015/503, Oak Ridge National Laboratory: Oak Ridge, TN, 2015.
(51) Chong, S.; Riley, B. J.; Asmussen, R. M.; Lawter, A. R.; Bruffey, S. H.; Nam, J.; McCloy, J. S.; Crum, J. V. Iodosodalite synthesis with hot isostatic pressing of precursors produced from aqueous and hydrothermal processes. *J. Nucl. Mater.* **2020**, *538*, No. 152222.
(52) Chong, S.; Peterson, J. A.; Riley, B. J.; Tabada, D.; Wall, D.; Corkhill, C. L.; McCloy, J. S. Glass-bonded iodosodalite waste form for immobilization of ^{129}I. *J. Nucl. Mater.* **2018**, *504*, 109.
(53) Riley, B. J.; Vienna, J. D.; Frank, S. M.; Kroll, J. O.; Peterson, J. A.; Canfield, N. L.; Zhu, Z.; Zhang, J.; Kruska, K.; Schreiber, D. K.; Crum, J. V. Glass Binder Development for a Glass-Bonded Sodalite Ceramic Waste Form. *J. Nucl. Mater.* **2017**, *489*, 42.
(54) Garino, T. J.; Nenoff, T. M.; Krumhansl, J. L.; Rademacher, D. X. Low-temperature sintering Bi-Si-Zn-oxide glasses for use in either glass composite materials or core/shell ^{129}I waste forms. *J. Am. Ceram. Soc.* **2011**, *94*, 2412.
(55) Lere-Adams, A. J.; Dixon Wilkins, M. C.; Bollinger, D.; Stariha, S.; Farzana, R.; Dayal, P.; Gregg, D. J.; Chong, S.; Riley, B. J.; Heiden, Z. M.; et al. Glass-bonded ceramic waste forms for immobilization of radioiodine from caustic scrubber wastes. *J. Nucl. Mater.* **2024**, *591*, No. 154938.
(56) Evarts, J. S.; Chong, S.; Oshiro, J. M.; Riley, B. J.; Asmussen, R. M.; McCloy, J. S. Ceramic−Metal (Cermet) Composites: A Review of Key Properties and Synthesis Methods Focused on Nuclear Waste Immobilization. *Ind. Eng. Chem. Res.* **2024**, *63*, 6003.
(57) Maddrell, E. R. *The Immobilisation of Mercury Containing Residues*, NNL(11)-11805, National Nuclear Laboratory: Sellafield, Cumbria, U.K., 2012.
(58) Evarts, J. S.; Chong, S.; Oshiro, J. M.; Riley, B. J.; Asmussen, R. M.; McCloy, J. S. Ceramic-Metal (Cermet) Composites: A Review of Key Properties and Synthesis Methods Focused on Nuclear Waste Immobilization. *Ind. Eng. Chem. Res.* **2024**, *63*, 6003.
(59) Riley, B. J. Electrochemical Salt Wasteform Development: A Review of Salt Treatment and Immobilization Options. *Ind. Eng. Chem. Res.* **2020**, *59*, 9760.

https://doi.org/10.1021/acsomega.4c03378
ACS Omega 2024, 9, 34661−34674

(60) Riley, B. J.; Garn, T., Purification of Gas and Liquid Streams Using Composite Sorbents Embedded in a Polyacrylonitrile Matrix, In*Advances in Materials Science Research*; Wythers, M., Ed.; Nova Science Publishers: 2019; Vol. *35*, p 119.
(61) Riley, B. J.; Chong, S.; Asmussen, R. M.; Bourchy, A.; Engelhard, M. H. Polyacrylonitrile Composites of Ag-Al-Si-O Aerogels and Xerogels as Iodine and Iodide Sorbents. *ACS Appl. Polym. Mater.* **2021**, *3*, 3344.
(62) Chong, S.; Riley, B. J.; Asmussen, R. M.; Fujii Yamagata, A.; Marcial, J.; Lee, S.; Burns, C. A. Iodine capture with metal-functionalized polyacrylonitrile composite beads containing Ag^0, Bi^0, Cu^0, or Sn^0 particles. *ACS Appl. Polym. Mater.* **2022**, *4*, 9040.
(63) Yu, Q.; Jiang, X.; Cheng, Z.; Liao, Y.; Pu, Q.; Duan, M. Millimeter-sized Bi_2S_3@polyacrylonitrile hybrid beads for highly efficient iodine capture. *New J. Chem.* **2020**, *44*, 16759.
(64) Yu, Q.; Jiang, X.; Duan, M. Nano-flower-shaped SnS_2 doped polyacrylonitrile hybrid beads for effective capture of radioactive gaseous iodine.*Soc. Sci. Res. Net.* **2021**.
(65) Riley, B. J.; Chong, S.; Kuang, W.; Varga, T.; Helal, A. S.; Galanek, M.; Li, J.; Nelson, Z. J.; Thallapally, P. K. Metal-organic framework-polyacrylonitrile composite beads for xenon capture. *ACS Appl. Mater. Interfaces* **2020**, *12*, 45342.
(66) Shetty, S.; Numkiatsakul, P.; Wickline, K.; Incarnato, R.; Wang, H.; Kunkel, H.; Randall, C. A.; Trolier-McKinstry, S. Development of Polymer-Ceramic-Metal Graded Acoustic Matching Layers via Cold Sintering. *IEEE Trans. Ultrason. Ferroelectr. Frequ. Contr.* **2022**, *69*, 1413.
(67) Guo, J.; Floyd, R.; Lowum, S.; Maria, J.-P.; Herisson de Beauvoir, T.; Seo, J.-H.; Randall, C. A. Cold Sintering: Progress, Challenges, and Future Opportunities. *Annu. Rev. Mater. Res.* **2019**, *49*, 275.
(68) Riley, B. J.; Canfield, N. C.; chong, S.; Oshiro, J. M.; George, J. L.; Burns, C. A.; Helgeland, J. L. *Evaluating Iodine Immobilization Technologies: Cermets, Polycermets, and Polyhalmets*, PNNL-35738, Pacific Northwest National Laboratory: Richland, WA, 2024.
(69) Vatanpour, V.; Pasaoglu, M. E.; Kose-Mutlu, B.; Koyuncu, I. Polyacrylonitrile in the Preparation of Separation Membranes: A Review. *Ind. Eng. Chem. Res.* **2023**, *62*, 6537.
(70) Liu, P. S.; Chen, G. F., Making Porous Metals, In *Porous Materials: Processing and Applications*; Liu, P. S.; Chen, G. F., Eds.; Butterworth-Heinemann (Elsevier): Amsterdam, 2014; p 43.
(71) Lide, D. R. *CRC Handbook of Chemistry and Physics*; 88th ed.; CRC Press: Boca Raton, FL, 2008.
(72) Khairulin, R. A.; Stankus, S. V.; Abdullaev, R. N.; Sklyarchuk, V. M. The density and interdiffusion coefficients of bismuth-tin melts of eutectic and near-eutectic composition. *High Temp.* **2010**, *48*, 188.
(73) Oshiro, J. M.; Fujii Yamagata, A.; Sharma, S.; Asmussen, R. M.; Chong, S.; Riley, B. J.; Crum, J. V.; Silverstein, J. A.; Lian, J. Pelletization with spark plasma sintering and characterization of metal iodides: An assessment of long-term radioiodine immobilization options. *Under review at Ind. Eng. Chem. Res.* **2024**.
(74) Riley, B. J.; Chong, S.; Beck, C. L. Iodine vapor reactions with pure metal wires at temperatures of 100−139 °C in air. *Ind. Eng. Chem. Res.* **2021**, *60*, 17162.
(75) MTI, 2023, *Calculating applied pressure on pellet pressing die*, https://www.mtixtl.com/YLJ-HP2-H.aspx.
(76) Riley, B. J.; Kroll, J. O.; Peterson, J. A.; Matyáš, J.; Olszta, M. J.; Li, X.; Vienna, J. D. Silver-loaded aluminosilicate aerogels as iodine sorbents. *ACS Appl. Mater. Interfaces* **2017**, *9*, 32907.
(77) Riley, B. J.; Chong, S.; Marcial, J.; Lahiri, N.; Bera, M. K.; Lee, S.; Wu, T.; Kruska, K.; Matyáš, J. Silver-loaded xerogel nanostructures for iodine capture: A comparison of thiolated versus unthiolated sorbents. *ACS Appl. Nano Mater.* **2022**, *5*, 9478.
(78) Chong, S.; Riley, B. J.; Kuang, W.; Olszta, M. J. Iodine capture with mechanically robust heat-treated Ag-Al-Si-O xerogel sorbents. *ACS Omega* **2021**, *6*, 11628.
(79) Riley, B. J. A multifunctional technology platform for sorbent construction using polyacrylonitrile scaffolds. *Ind. Eng. Chem. Res.* **2024**, *63*, 8647.
(80) Reiser, J. T.; Lawter, A. R.; Avalos, N. A.; Bonnett, J.; Riley, B. J.; Chong, S.; Canfield, N.; Saslow, S. A.; Bourchy, A.; Asmussen, R. M. Review and experimental comparison of the durability of iodine waste forms in semi-dynamic leach testing. *Chem. Eng. J. Adv.* **2022**, *11*, No. 100300.
(81) Wagner, B.; Huttner, A.; Bischof, D.; Engel, A.; Witte, G.; Heine, J. Chemical Surface Reactivity and Morphological Changes of Bismuth Triiodide (BiI_3) under Different Environmental Conditions. *Langmuir* **2020**, *36*, 6458.
(82) Yang, J. H.; Cho, Y.-J.; Shin, J. M.; Yim, M.-S. Bismuth-embedded SBA-15 mesoporous silica for radioactive iodine capture and stable storage. *J. Nucl. Mater.* **2015**, *465*, 556.
(83) Vance, E. R.; Grant, C.; Karatchevtseva, I.; Aly, Z.; Stopic, A.; Harrison, J.; Thorogood, G.; Wong, H.; Gregg, D. J. Immobilization of iodine via copper iodide. *J. Nucl. Mater.* **2018**, *505*, 143.
(84) Riley, B. J.; Turner, J.; McFarlane, J.; Chong, S.; Carlson, K.; Matyas, J. Design of iodine solid sorbents for iodine: A literature review of the critical criteria for consideration. *Under review atMater. Adv.* **2024**.
(85) Robinson, A. J.; Johnson, H. M.; Chong, S.; Riley, B. J.; Murphy, M. K.; Okabe, P.; Thallapally, P. K. Noble gas management with radiation-tolerant MOF for molten salt reactors. *Cell Rep. Phys. Sci.* **2024**, *5*, No. 101829.

https://doi.org/10.1021/acsomega.4c03378
ACS Omega 2024, 9, 34661−34674